Figure S1. Sampling locations before (a) and after (b) EDM for X-ray microtomography (1), Raman spectroscopy, AFM and TG/DSC (2), and nanoindentation and SEM (3).....2
Table S1. Acquisition, reconstruction, calibration, and data-treatment parameters for X-ray computed microtomography 3
Figure S2. Xradia Versa 520 X-ray microtomography system used in the laboratory 5
Figure S3. ATR 8000 Raman spectrometer used in the laboratory.....6
Table S2. Raman spectroscopy measurement protocol.....6
Figure S4. Thermoscan-2 instrument used in the laboratory.....7
Figure S5. NanoTest 600 Platform 3 instrument used in the laboratory 7
Table S3. TG/DSC results for the polymer core before and after EDM 8
Supplementary S. Model Verification and Sensitivity Analysis.....9
Supplementary S1. Equations and Problem Conditions.....9
Supplementary S2. Nomenclature and Parameter Provenance.....10
Supplementary S3. Measurement Locations and Uncertainty Sources.....11
Supplementary S4. Fitting and Quantitative Comparison 12
Supplementary S5. Verification of the Diagnostic Thermal Problem 13
Supplementary S6. Material and Time Verification of Die-Sinking.....13
Supplementary S7. Sensitivity to Coefficients and Energy Inputs.....13
Supplementary S8. Reproduction and Limits of the Conclusions 14
Supplementary S9. Electrode Fabrication Cost Calculation.....15
S9.1. Geometry and Material Components of the SLA Route.....15
S9.2. Initial Bath Charges.....15
S9.3. Allocation of Material Costs.....16
S9.4. Solid-Copper Electrode and Machining.....17
S9.5. Comparison of Fabrication Routes 17
S9.6. Sources of Prices and Material Properties 17

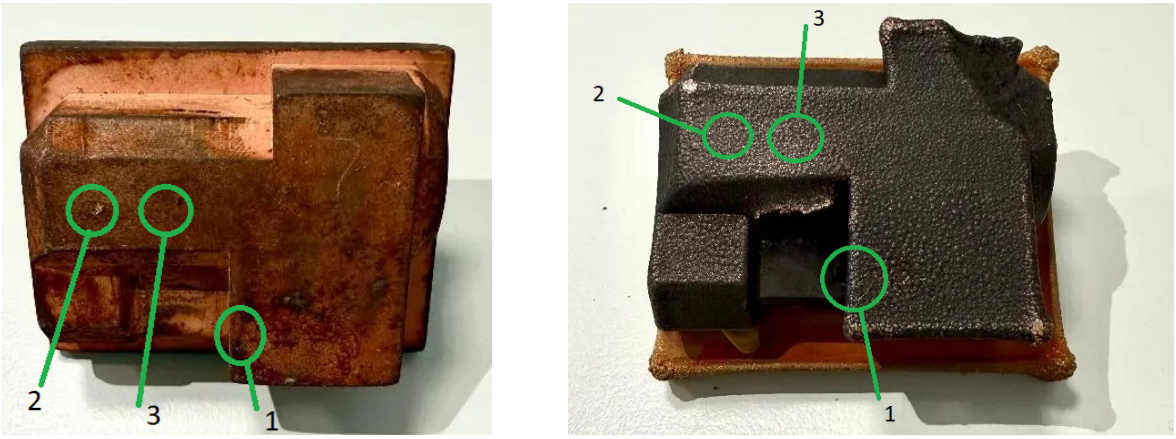


Figure S1. Sampling locations before (a) and after (b) EDM for X-ray microtomography (1), Raman spectroscopy, AFM and TG/DSC (2), and nanoindentation and SEM (3).

Table S1. Acquisition, reconstruction, calibration, and data-treatment parameters for X-ray computed microtomography

Parameter	Description
Instrument	Xradia Versa 520 X-ray microtomography system (Carl Zeiss X-ray Microscopy, Inc., Pleasanton, USA)
X-ray tube voltage	110 kV
X-ray source power	8.0 W
Objective	0.4×
Acquisition range	360° rotation
Number of projections	2401
Exposure time	4.0 s per projection
Primary acquisition filter	HE3 filter
Additional physical filter	HE5 filter, used to reduce ring artifacts
Source-to-rotation-axis distance	39.07 mm
Detector-to-rotation-axis distance	139.88 mm
Detector	2048 × 2048 pixel CCD camera maintained at −59 °C
Binning and projection dimensions	Binning factor of 2; projection images up to 1024 × 1024 pixels
Reconstructed voxel size	15.04 μm
Physical specimens	One copper-coated polymer specimen
Number of scans	One
Sampling region / region of interest	Central specimen segment containing the coating–substrate interface; the visualizations covered the coating–substrate system or a coating-focused displayed volume
Laboratory environment	Laboratory room temperature approximately 24 °C; temperature inside the micro-CT enclosure was not independently monitored
Geometric calibration	X-ray source–detector geometric alignment calibrated regularly
Object-imaging calibration	Calibration performed using a spherical reference specimen of known diameter
Projection reconstruction software	XRMReconstructor, version 12.0.8086.19558
Center-shift selection	Manually selected value of 21.1 to minimize reconstruction artifacts, focusing on the central specimen segment containing the coating–substrate interface
Beam-hardening correction	Parameter value of 0.075
Gaussian filtering	Gaussian blur filter, $\sigma = 0.7$
Drift compensation	Sample drift compensated for during acquisition and during reconstruction/post-processing
Visualization software	VGSTUDIO MAX 3.5
Grayscale classification	Manual selection of grayscale intensity ranges based on the reconstructed attenuation histogram; ranges used for Figure 11a are shown in that figure

Parameter	Description
Visualization 1	Coating, polymer substrate, and interfacial transition region displayed using different assigned colors (Figure 11a)
Visualization 2	Polymer substrate excluded from the displayed volume to focus on the coating morphology and adjacent interfacial region (Figure 11b)
Quantitative segmentation	Not performed; grayscale classification was used for qualitative visualization only
Threshold-sensitivity analysis	Not performed because quantitative phase segmentation and quantitative defect or porosity measurements were not conducted
Quantitative outputs	Phase-volume fractions, porosity values, and defect volumes were not calculated
Interpretation / acceptance criteria	Qualitative interpretability of the coating, substrate, interfacial region, and visible structural features at the method's spatial resolution; no formal quantitative acceptance criteria were established
Replication and limitations	One physical specimen and one scan; both visualizations were derived from the same reconstructed dataset and are not independent replicates



Figure S2. Xradia Versa 520 X-ray microtomography system used in the laboratory



Figure S3. ATR 8000 Raman spectrometer used in the laboratory

Table S2. Raman spectroscopy measurement protocol

Protocol item	**Description**
Instrument	ATR 8000 Raman spectrometer, OPTOSKY, China
Excitation and spectral range	Excitation wavelength: 785 nm; Raman-shift range: 160-3600 cm^{-1}
Acquisition parameters	– Power at the specimen: 300 mW – Exposure time: set automatically by the instrument
Specimen dimensions/mass	Not recorded; measurements were performed directly on solid specimens
Environmental conditions	– Measurement temperature: 25 °C – Relative humidity: not controlled – Atmosphere: air
Data processing	Baseline correction: applied. Smoothing: not applied.



Figure S4. Thermoscan-2 instrument used in the laboratory



Figure S5. NanoTest 600 Platform 3 instrument used in the laboratory

Table S3. TG/DSC results for the polymer core before and after EDM

Specimen	Mass, g		Residue at 800 °C, %
	Before	After*	
Before EDM	0.152	0.001	0.66
After EDM	0.124	0.001	0.81

Supplementary S. Model Verification and Sensitivity Analysis

This Supplementary provides the conditions of the main calibrated model at 220 ms, the numerical-verification protocol and the two parameter-identification stages. The diagnostic thermal problem is described separately from the integral removal law. Supplementary S3 gives reconstructed coordinates and metrological limitations; S4 explains the roles of the observations and limits of identifiability.

Supplementary S1. Equations and Problem Conditions

Deposition. The electrolyte satisfies $\nabla^2 u = 0$. The normal n points outward from the electrolyte domain. At the cathode, $\kappa \partial u/\partial n = -i$; on insulating walls and the masked shank, $\partial u/\partial n = 0$. At the anodes, $u = Ua$, where Ua is determined together with the total-current condition. The metallic cathode potential is zero; u is referenced to the Cu^{2+}/Cu equilibrium potential. The implemented kinetics are:

$$i = i_0[exp(\alpha cFu/RT) - exp(-\alpha aFu/RT)] / [1 + (i_0/iL)exp(\alpha cFu/RT)] \quad (1)$$

$$\Sigma_j i_j S_j = iav\Sigma_j S_j; \quad h_j = \varepsilon M i_j tdep / (2F\rho Cu) \quad (2)$$

The limiting current follows $iL = 2FDcbSh/L$, $Sh = 0.67(ScGr)^{1/4}$, $Sc = \nu/D$ and $Gr = g(\Delta\varrho/\varrho)L^3/\nu^2$. The BEM system uses collocation at the centroids of constant triangular elements and a damped Newton method; the implemented residual-norm criterion is $10^{-10}\sqrt{N}$. A Tafel solution at the mean current provides the initial estimate. Geometry remains fixed during deposition.

The main die-sinking calculation uses the integral law (10)–(11), normal wear (12)–(14), removal distribution (15) and common time budget (16). Initially, zw = 0 and the tool carries the initial BEM coating. The normal-layer state changes at every step; the external envelope is rebuilt every 200 s. The minimum geometric gap is maintained to conductive regions. Quadrature volume portions are not individual physical discharges.

The diagnostic thermal problem uses an axisymmetric energy equation and specific mass enthalpy H. Latent heat of fusion applies to the metals; polymer chemical kinetics are not specified. Boiling is allowed only at the current free surface, rather than throughout the volume of the fixed mesh:

$$\rho \frac{\partial H}{\partial t} = \frac{1}{r}\frac{\partial}{\partial r}\left(rk\frac{\partial T}{\partial r}\right) + \frac{\partial}{\partial z}\left(k\frac{\partial T}{\partial z}\right) \quad (3)$$

$$H = c(T - T_0) + L_m f_l(T), T \le T_b, P_{ev} \ge 0, (T_b - T)P_{ev} = 0 \quad (4)$$

Initially, $T = T_0 = 298.15$ K. At the axis, $\partial T/\partial r = 0$; at distant boundaries, $T = T_0$. Temperature and normal heat flux are continuous at an ideal copper–polymer contact. During heating, the Gaussian flux is $4.45\varphi UI \exp(-4.5r^2/R^2)/(\pi R^2)$; after switching off, heat is transferred to the dielectric with a coefficient of 2000 W/(m²·K). The anode-spot radius is $R(t) = 2.04 \times 10^3 I^{0.43} t^{0.44}$ μm for t in seconds, and the cathode-spot radius is 10 μm. These quantities were not reconstructed from measured waveforms.

An implicit finite-volume enthalpy scheme is used. The phase transition is smoothed over 20 K, and harmonic thermal resistance is applied at the layer interface. For the diagnostic 220 ms calculation, the domain size is 30 mm and initial cell sizes are 1 μm radially and 0.5 μm in depth. Surface motion limits the adaptive time step. Excess surface energy is assigned to latent heat of vaporization; removed material also carries

sensible and phase enthalpy. At switch-off, a selected fraction of the current surface-connected melt is removed, rather than the envelope of all previously molten regions.

$$E_{in} = E_{stored} + E_{boundary} + E_{vapour} + E_{liquid} + R_E \quad (5)$$

Upon axial exposure of the base, heating of both electrodes is stopped simultaneously in the diagnostic solver. This is a separate hypothesis for termination of a local discharge. Geometry and conductive facets are rebuilt after surface recession. Diagnostic temperatures and volumes do not replace the calibrated integral law of the main run and do not establish a protective coating thickness.

Supplementary S2. Nomenclature and Parameter Provenance

Table 1. Parameters

Symbol	Quantity	Units	Value and status
αc; ε	Effective deposition parameters	1	1.7204; 0.7957; fitted to locations 4–10
κ; i_0; αa	Conductivity and kinetics	S/m; A/m²; 1	20; 10; 1.5; reference/adopted values
iav; tdep	Deposition	A/m²; h	300; 32; fabrication conditions
D; cb; ν	Diffusion, concentration and viscosity	m²/s; mol/m³; m²/s	5.3×10^{-10}; 881; 1.2×10^{-6}; input estimates
L; Δϱ/ϱ	Natural convection	mm; 1	20; 0.10; prescribed inputs
I; ton	Discharge	A; ms	8.1; 220; operator report; 0.220 s in the model
U; toff; td	Burning voltage, off time and delay	V; μs; μs	25; 80; 20; prescribed model inputs
φw; φCu; ηp	Power and operating fractions	1	0.18; 0.18; 1; prescribed main-model inputs
Rcat; hd	Cathode spot and cooling	μm; W/(m²·K)	10; 2000; diagnostic thermal problem only
ϱ; c; k; Tm; Lm; Tb; Lv	Material properties	SI	Table 11; reference values for metals
Tg; Tdeg	Polymer reference values	°C	90: estimated; approximately 280: TGA onset
gb; δ; λ; s	Gap geometry	μm	60; 30; 15; 115; geometric inputs
kw; vn; Δ	Steel removal, normal wear and grid spacing	1; μm/h; mm	0.15273; 65.724; 0.10; two coefficients calibrated to locations 1–3
Contact rule	Loss of support and flaking	Geometric condition	Zero resistance of exposed polymer on contact with steel; not a strength law

Physical constants are F = 96485.33 C/mol, R = 8.314462 J/(mol·K) and MCu = 0.063546 kg/mol. Effective-parameter sensitivity is assessed over αc = 1.5483–1.8924 and

ε = 0.7162–0.8753, corresponding to ±10% variation. No confidence level is assigned to these ranges, and statistical intervals were not estimated from the available data. Varying ε scales thickness linearly, whereas αc changes the current distribution.

Supplementary S3. Measurement Locations and Uncertainty Sources

Table 1. Measurement locations and uncertainty sources

Location	Surface	X; Y; Z, mm	h after EDM, μm	Role
1	End face	6.01; -8.00; -14.50	792.1	EDM calibration
2	Chamfer	12.99; -8.00; -12.61	1007.7	EDM calibration
3	Wall, 9.9 mm	14.60; -8.00; -9.91	898.2	EDM calibration
4	Wall, 5.6 mm	14.60; -8.00; -5.64	616.1	Fitting
5	Wall, 3.1 mm	14.60; -8.00; -3.07	454.3	Fitting
6	Wall near the inner corner	14.60; -8.00; -0.83	264.6	Fitting
7	Shelf near the inner corner	15.26; -8.00; 0.00	293.4	Fitting
8	Shelf center	18.28; -8.00; 0.00	616.0	Fitting
9	Plate rib	20.10; -8.00; 0.00	1220.6	Fitting
10	Plate edge	20.10; -8.00; 0.68	1224.5	Fitting

Coordinates are reconstructed in the STL coordinate system, with the working end face of the base at Z = −14.5 mm. The displayed decimal places describe the digital registration and do not establish positioning accuracy. One local thickness value is reported per location. The ten locations characterize the spatial distribution in a cross-section of one electrode.

Table 2. Spatial distribution in a cross-section of one electrode

Component	Data needed to evaluate the contribution	Available information
Image scale	Stage-micrometer calibration, magnification and scale-bar source	2000 μm scale bar present; independent calibration undocumented
Boundary positions	Repeated boundary identification and inter-operator variation	No repeated local readings
Cross-section preparation	Tilt, edge rounding and deformation from cutting/grinding	Preparation procedure described; numerical contribution not determined
CAD registration	Section-plane and point positions; thickness-gradient effects	Digital reconstruction; coordinate uncertainty not quantified
Initial geometry	Paired pre-deposition dimensions and a pre-EDM cross-section	Initial local working-surface thickness not independently measured

For the measurement model $h = a \cdot l$, where a is scale in μm/pixel and l is boundary separation in pixels, independent contributions give $u^2(h) = l^2u^2(a) + a^2u^2(l) + u^2\text{section} + u^2\text{location}$. Covariance terms are included in the general case [32]. At approximately 24.4

μm/pixel, rounding each boundary position within ±0.5 pixel gives u ≈ 24.4/√6 ≈ 10 μm. This estimate applies only to pixel reading. A complete numerical budget and expanded uncertainty were not determined: independent scale calibration, repeated local readings and the cross-section-preparation contribution were not quantified. Full measurement uncertainty and probabilistic prediction intervals are therefore not reported for the ten locations.

Supplementary S4. Fitting and Quantitative Comparison

Table 1. Quantitative comparison

Location	h after EDM, μm	Modeled h_0, μm	$h_0 - h$, μm	h_0 range, μm	Experimental u, μm
1	792.1	1089.7	297.6	978.5–1201.6	Not evaluated
2	1007.7	1208.7	201.0	1086.9–1330.1	Not evaluated
3	898.2	971.3	73.1	874.1–1068.6	Not evaluated
4	616.1	574.1	-42.0	510.0–641.2	Not evaluated
5	454.3	418.7	-35.6	367.9–473.4	Not evaluated
6	264.6	300.9	36.3	260.0–346.1	Not evaluated
7	293.4	285.4	-8.0	245.8–329.5	Not evaluated
8	616.0	605.5	-10.5	539.0–674.6	Not evaluated
9	1220.6	1276.1	55.5	1132.3–1422.0	Not evaluated
10	1224.5	1254.3	29.8	1114.7–1395.7	Not evaluated

The h_0 range is formed from nine combinations of αc and ε at −10%, 0 and +10%, without refitting. It describes sensitivity of the initial deposition field and is neither a final-thickness interval nor a probabilistic interval. The $h_0 - h$ column contains a model-dependent difference and is not entered into the objective as independently measured wear. Locations 4–10 determine deposition, and locations 1–3 determine the EDM parameters. Final residual thicknesses and their calibration errors are given in Tables 10 and 14.

The protocol distinguishes BEM checks against analytical problems and mesh refinement; verification of the diagnostic thermal implementation; die-sinking checks on material, time and discretization; deposition calibration using locations 4–10; and EDM calibration using locations 1–3 with a step-engagement constraint. Logarithms of positive parameters are used. Search ranges kw = 0.02–0.40 and vn = 5–250 μm/h are not confidence intervals. Even full rank of the local sensitivity matrix refers to fixed U, φ and engagement law: the same steel removal rate is retained with kw′ = kwU/U′. All ten observations are calibration data. Independent assessment requires a separate experiment with coefficients fixed in advance and measurements of initial and residual coating, cavity geometry and removed steel.

Supplementary S5. Verification of the Diagnostic Thermal Problem

Checks cover the analytical linear limit without melting, metal phase energy, finite evaporating coating inventory, removal of full enthalpy with eroded material and consistent termination of local heating upon axial exposure. These checks are included in the automated test suite. They verify the implementation of the diagnostic hypothesis rather than the actual experimental pulse shape or interface temperature.

The diagnostic thermal problem tests hypotheses about a local discharge. MRR in the main model is determined by the integral law; thermal-solver outputs are not used as input crater volumes. Numerical verification of the main die-sinking calculation and coefficient sensitivity are given in S6–S7 and Tables 15–16.

Supplementary S6. Material and Time Verification of Die-Sinking

The full run ends exactly at 16,200 s. Frontal and lateral removal consume the same $Q_w \Delta t$ budget. Steel volume is compared with the integrated height-map change; copper loss is compared with the reference-facet inventory difference and the sum of erosion and flaking. Initial copper inventory is 7042.516 mm^3 and final inventory is 6628.346 mm^3, giving a loss of 414.169 mm^3. Flaking is zero in the main run and is accounted for separately from normal erosion.

The steel residual is 1.02×10^{-10} mm^3 and the copper-loss partition residual is 4.96×10^{-11} mm^3. Normal erosion cannot exceed the inventory of a facet, and geometric rounding creates no additional copper. Monotonic external-envelope recession and normal thinning of vertical walls are checked. Frame-saving frequency and random selection of visualization points do not change the main solution.

Table 15 covers grid spacings of 0.20, 0.15 and 0.10 mm, geometry-update periods of 600, 200 and 100 s, and halving of the adaptive time step. Coefficients are not refitted for each mesh. The location and volume of local contact failure remain grid-sensitive; numerical testing does not establish tool life or measured repeatability.

Supplementary S7. Sensitivity to Coefficients and Energy Inputs

Table 16 and Figure 23 show calculations with kw and vn varied by ±10% without refitting. At kw −10% and +10%, calculated depths are 7.840 and 9.015 mm. At vn −10% and +10%, working end-face residual thicknesses are 831.8 and 774.5 μm. These are deterministic sensitivities rather than probabilistic prediction intervals.

In the integral law, Q_w is proportional to $k_w \varphi_w U \delta \eta p$. Changing U and φ_w at fixed kw changes the removal rate; refitting kw can compensate for the scale change. The prescribed values of 25 V and 0.18 are therefore not independently determined from residual thicknesses. Replacing U = 25 V with 20 V preserves the rate when $k_w' = k_w \cdot 25/20$. This illustrates non-uniqueness rather than an additional experimental estimate.

The off time of 80 μs and delay of 20 μs are prescribed inputs. For 220 ms, the nominal discharge-on fraction is 0.999546, frequency is 4.5434 Hz and energy at 25 V and 8.1 A is 44.55 J per nominal cycle. These quantities are not identified with recorded

waveforms. The available data do not reconstruct local spot lifetime or the internal generator structure.

Supplementary S8. Reproduction and Limits of the Conclusions

Main commands from the package root are: python run.py simulate presets/article_220ms_calibrated.toml; python review_work/fit_surface_model.py; python review_work/verify_surface_model.py; python -m pytest tests -q. Package versions are listed in requirements-review.txt. The package includes the fixed BEM mesh with the initial-layer field and the calibration-script inputs. File SHA-256 checksums are provided in manifest.json. The full animation frames are regenerated by the main run.

Verification and sensitivity analysis apply to the selected geometry, prescribed energy inputs and calibrated normal-wear law. Numerical repetitions do not establish statistical independence or reproducibility between electrodes. A full measurement budget and independent initial working-surface thicknesses are unavailable. Independent experimental validation of MRR, depth and tool life remains outstanding; residual-thickness fitting accuracy does not transfer to those outputs.

Supplementary S9. Electrode Fabrication Cost Calculation

The calculation covers two electrode-fabrication routes: SLA printing of a polymer base followed by electroless and electrochemical copper plating, and milling of solid copper. Geometric quantities are calculated from models/electrode_real.stl in the reproducibility package. All monetary amounts are expressed in USD. Catalog prices recorded on 18 October 2026 are converted at the Bank of Russia rate applicable on 19 October 2026: USD 1 = RUB 83.6177, effective from 17 October 2026 [14].

S9.1. Geometry and Material Components of the SLA Route

The volume of the closed STL mesh, calculated by summing oriented tetrahedral volumes, is 29.413734 cm^3. Model dimensions are 40.2 × 50.0 × 39.5 mm. Resin consumption is calculated as mres = kresϱresV, where ϱres = 1.17 g/cm^3 is the liquid density of Industrial High Temp resin from the manufacturer technical data sheet [2], and kres = 1.0–1.5 accounts for supports and process losses. The digital-base volume is used without a separate shrinkage correction. Resin mass is 34.414–51.621 g.

Initial copper volume is taken from the coating model as the sum of reference-facet areas multiplied by local initial thicknesses: VCu = ΣAjhj = 7.043 cm^3. At 8.93 g/cm^3, the corresponding mass is 62.890 g. This is metal contained in the coating; additional anode consumption depends on process losses. The quantity is the initial copper inventory in results/article_220ms_calibrated/summary.json.

At a resin price of USD 118.40/kg [1], resin cost is USD 4.07–6.11. An M1 anode price of USD 34.47/kg [3] gives USD 2.17 for coating copper. The combined cost is USD 6.24–8.28. Cost is allocated in proportion to the quantity of material used.

S9.2. Initial Bath Charges

The preparation and activation charges are 0.2 L of 20 wt.% NaOH; 0.2 L of a solution containing $SnCl_2 \cdot 2H_2O$ at 40 g/L and HCl at 40 mL/L; and 0.2 L of $AgNO_3$ at 1 g/L. The 1 L electroless copper bath contains 20 g $CuSO_4 \cdot 5H_2O$, 20 g Rochelle salt, 10 g Na_2SO_4, 10 g NaOH and 20 g formalin. The 1 L electroplating bath contains 220 g $CuSO_4 \cdot 5H_2O$ and 60 g H_2SO_4. Formalin is treated as a commercial solution containing 37–40% formaldehyde.

Commercial-reagent masses are calculated using a density of 1.20 g/mL for 20 wt.% NaOH, 1.19 g/mL for concentrated HCl, and an H_2SO_4 mass fraction of 0.94. Thus, 0.2 L of NaOH solution requires 48 g of solid reagent; the HCl charge is 8 mL (9.52 g), and the commercial H_2SO_4 solution mass is 60/0.94 = 63.83 g.

Table S9.1. Reagent cost of the initial bath charges

Reagent	Quantity	Unit price, USD/kg	Cost, USD / source
NaOH for pretreatment and electroless plating	48 + 10 g	12.55	0.73 / [4]
$SnCl_2 \cdot 2H_2O$ for 0.2 L of solution	8 g	77.47	0.62 / [5]
Concentrated HCl solution	8 mL ≈ 9.52 g	3.76	0.04 / [6]
$AgNO_3$ for 0.2 L of solution	0.2 g	3326.57	0.67 / [7]
$CuSO_4 \cdot 5H_2O$ for electroless and electroplating baths	20 + 220 g	22.25	5.34 / [8]
Rochelle salt	20 g	18.97	0.38 / [9]
Anhydrous Na_2SO_4	10 g	4.78	0.05 / [10]
Commercial concentrated H_2SO_4	60/0.94 = 63.83 g	3.12	0.20 / [11]
Formalin, 37–40%	20 g of solution	0.96	0.02 / [12]
Initial charge K_0	Excluding water and washing	—	8.03

Reagent prices are normalized to kilograms using the listed package sizes. The Rochelle-salt quotation is USD 7.77 per 0.5 kg before the seller-specified 22% VAT [9]; VAT is included in its tabulated cost. Other prices are used as published. Copper stock, anode and milling-rate values include VAT. Delivery, minimum-order charges and discounts are excluded. The experimental reagent suppliers and the catalog sources used for price inputs are distinguished in Table S9.4. Totals are calculated from unrounded values and rounded to two decimal places.

K_0 is the cost of the initial inventory of the selected reagents. Water, washing liquids, isopropanol, filters and subsequent replenishment are separate cost items. Coating copper is accounted for in S9.1. The initial $CuSO_4$ charge describes the inventory in the solution and does not replace accounting for the dissolving anode.

S9.3. Allocation of Material Costs

The material subtotal per fabrication operation is calculated as Cmat,SLA = kresϱresVpres + mCupan + K_0/N. Here pres and pan are the resin and anode-copper unit prices, and N is the number of operations over which the initial charge is allocated. Dependence on inventory allocation is evaluated for N = 1, 10 and 50, with zero recovered value for the remaining charge. If a recovered value R is included, the last term becomes (K_0 − R)/N. Replenishment and bath maintenance are separate items.

Table S9.2. Material cost components of SLA printing and copper plating

N	Resin and Cu, USD	Reagent allocation K_0/N, USD	Material subtotal, USD
1	6.24–8.28	8.03	14.28–16.31
10	6.24–8.28	0.80	7.05–9.08
50	6.24–8.28	0.16	6.40–8.44

Table S9.2 includes only the stated materials and allocated initial charge. Complete fabrication cost also includes energy, active labor, equipment occupancy and depreciation, finishing, inspection, replenishment, process losses and waste handling. Cost per acceptable electrode additionally depends on the acceptable-electrode yield Y. The 32 h electroplating duration is process-cycle time and is distinguished from operator labor time.

S9.4. Solid-Copper Electrode and Machining

A solid-copper body reproducing the same STL model has a mass $m_{Cu,solid} = \varrho_{Cu} V = 262.665$ g. The milling blank is 50 × 55 × 45 mm, with a volume of 123.75 cm³ and mass of 1.105087 kg. Machining to the STL geometry removes 94.336 cm³, corresponding to 842.4 g.

The blank is valued at USD 35.79/kg for 30–60 mm-thick M1 copper stock in the 0–50 kg category of the 15 October 2026 price list [3], giving USD 39.55 per blank. Milling is calculated using a published starting rate of USD 29.90/h including VAT [C13]. The subtotal $C_{Cu,mill} = m_{stock} p_{M1} + r_{mill} t_{mill}$ is evaluated at t_{mill} = 1, 2 and 4 h. These times are parameters of the cost calculation.

Table S9.3. Solid-copper blank and milling cost

tmill, h	Blank, USD	Milling, USD	Blank and milling, USD
1	39.55	29.90	69.45
2	39.55	59.80	99.34
4	39.55	119.59	159.14

Table S9.3 excludes stock cutting and delivery, process planning and CAM programming, fixtures and setup where charged separately from the machine rate, finishing and inspection. Recovered chip value is zero in the tabulated calculation; where applicable, the product of recovered chip mass and its resale price is subtracted. Blank size and workholding are finalized during process planning, while machine time depends on tools, cutting parameters, toolpaths and surface requirements.

S9.5. Comparison of Fabrication Routes

Both routes use the STL model of the polymer base as their geometric reference. The same final working surface requires allowance for copper coating, finishing and spark-gap compensation. Modeled coating-copper inventory and solid-copper part volume characterize material quantities on this common geometric basis.

Tables S9.2 and S9.3 cover different sets of production operations: SLA and plating materials in the former, and stock plus milling in the latter. A comparison of complete costs requires the corresponding preparation, fabrication and inspection operations in both calculations. Workpiece machining costs also depend on tool life, electrode and replacement counts, EDM time, finishing and acceptable-part yield. The subtotals describe cost structure without establishing a percentage saving or comparative tool life.

S9.6. Sources of Prices and Material Properties

Material price quotations were recorded on 18 October 2026; the copper price list is dated 15 October 2026. USD amounts use the Bank of Russia rate applicable on 19 October 2026, USD 1 = RUB 83.6177, effective from 17 October 2026 [14]. Experimental suppliers in Sections 2.2 and 2.3 identify the reagents actually used. Sources 4–12 identify

the catalog vendors whose quotations provide price inputs; these are distinct from experimental batch-purchase records. Table S9.4 records both roles. Quantities and formulations are given in S9.1–S9.4.

Table S9.4. Experimental reagent suppliers and catalog price inputs

Reagent	**Experimental supplier in Sections 2.2–2.3**	**Catalog source used for pricing**
NaOH	VEKTON for pretreatment; not separately specified for the electroless bath	VEKTON [4]
$SnCl_2 \cdot 2H_2O$; HCl	Not specified	VEKTON [5, 6]
$AgNO_3$	LENREACTIV; chemically pure	VEKTON; analytical grade [7]
$CuSO_4 \cdot 5H_2O$	KHIMREAKTIVSNAB in Section 2.2; not separately specified in Section 2.3	VEKTON; analytical grade [8]
Rochelle salt	KHIMREAKTIV-74; analytical grade	Khimicheskie Resheniya; analytical grade [9]
Na_2SO_4	Baza No. 1 Khimreaktivov; chemically pure	ChemStore; 99% [10]
H_2SO_4	Sigma Tek; chemically pure	VEKTON; chemically pure [11]
Formalin	LENREACTIV; technical grade	Khimservice; 37–40% solution [12]

Experimental supplier websites: VEKTON; LENREACTIV; KHIMREAKTIVSNAB; Baza No. 1 Khimreaktivov; Sigma Tek

[1] HARZ Labs. Industrial High Temp resin. USD 118.40/kg. https://harzlabs.ru/products/materialy/industrial-high-temp.html

[2] HARZ Labs. Industrial High Temp technical data sheet, V6.0, 4 February 2025. Liquid density 1.17 g/cm³. https://harzlabs.com/upload/iblock/8d7/1c99q7vcf6jnir91diy62us0ri25b81i/TDS-Industrial-High-Temp-Resin-V6.0-eng.pdf

[3] Galaktika. Price list dated 15 October 2026. M1 anode: USD 34.47/kg; M1 stock, 30–60 mm: USD 35.79/kg. Quantity category 0–50 kg; VAT included. https://spb.galakmet.ru/upload/galaktika_spb.pdf

[4] VEKTON. Analytical-grade NaOH. USD 1.25 per 0.1 kg. Price input for NaOH. https://vekton.ru/catalog/detail/natriy-gidrookis-chda-0-1kg/

[5] VEKTON. Analytical-grade $SnCl_2 \cdot 2H_2O$. USD 38.74 per 0.5 kg. Catalog price input. https://vekton.ru/catalog/detail/olovo-khlorid-ii-2-vodnoe-imp-chda-0-5-kg/

[6] VEKTON. High-purity HCl, grade 20-4. USD 4.52 per 1.2 kg. Catalog price input. https://vekton.ru/catalog/detail/solyanaya-kislota-osch-20-4/

[7] VEKTON. Analytical-grade $AgNO_3$. USD 166.33 per 50 g. Price input; the experimental reagent was supplied by LENREACTIV. https://vekton.ru/catalog/detail/serebro-azotnokisloe-chda-50-gr/?oID=31121

[8] VEKTON. Analytical-grade $CuSO_4 \cdot 5H_2O$. USD 2.23 per 0.1 kg. Price input; Section 2.2 identifies KHIMREAKTIVSNAB for the experimental reagent. https://vekton.ru/catalog/detail/med-sernokislaya-ii-5-vodnaya-chda-0-1kg/

[9] Khimicheskie Resheniya. Analytical-grade Rochelle salt. USD 7.77 per 0.5 kg before seller-specified 22% VAT. Price input; the experimental supplier is KHIMREAKTIV-74. https://www.csdb.ru/shop/himicheskie-reaktivy/kalij-natrij/kalij-natrij-vinnokislyj/503002/

[10] ChemStore. Anhydrous Na_2SO_4, 99%. USD 4.78/kg. Price input; the experimental supplier is Baza No. 1 Khimreaktivov. https://chemstore.spb.ru/catalog/khimicheskie-reaktivy/natriy-sernokislyy-bezvodnyy.html

[11] VEKTON. Chemically pure H_2SO_4. USD 5.75 per 1.84 kg. Price input; the experimental supplier is Sigma Tek. https://vekton.ru/catalog/detail/sernaya-kislota-khch/

[12] Khimservice. Formalin, 37–40%. USD 0.96/kg, canister supply, VAT included. Price input; the experimental supplier is LENREACTIV. https://himservise.ru/catalog/p/formalin/

[13] Metalloobrabotka-ZR. Copper-part manufacture. Published starting milling rate: USD 29.90/h including VAT. https://metalloobrabotka.org/izgotovlenie-detaley-iz-medi

[14] Bank of Russia. Official USD exchange rate applicable on 19 October 2026: USD 1 = RUB 83.6177, effective from 17 October 2026. https://www.cbr.ru/scripts/XML_daily.asp?date_req=19/10/2026